THE 3-D PERFORMANCE IMPROVEMENT OF PHOTOVOLTAIC SYSTEMS WITH PCM AND FIN-BASED COOLING

by

Ahmed RETERI[a], Nabil Abdel Illah KORTI[a], Younes MENNI[b,c], Mustafa BAYRAM[d*], Omolayo M. IKUMAPAYI[e], Abiodun BAYODE[e], Tin Tin TING[f,g], and Salih OZER[h]

[a] Department of Mechanics, ETAP Laboratory, University of Tlemcen, Tlemcen, Algeria
[b] Department of Mechanical Engineering, Institute of Technology,
University Center Salhi Ahmed Naama, Naama, Algeria
[c] College of Technical Engineering,
National University of Science and Technology, Dhi Qar, Iraq
[d] Department of Computer Engineering, Biruni University, Istanbul, Turkey
[e] Department of Mechanical Engineering, Northwest University, Potchefstroom, South Africa
[f] Faculty of Data Science and Information Technology,
INTI International University, Nilai, Malaysia
[g] School of Information Technology, UNITAR International University, Selangor, Malaysia
[h] Head of the Mechanical Engineering Department, Mus Alparslan University, Mus, Turkey

Original scientific paper
https://doi.org/10.2298/TSCI2504097R

Photovoltaic cell efficiency is notably affected by temperature, with higher operating temperatures leading to significant drops in electrical performance. To mitigate this thermal drawback, the present study investigates a passive cooling approach that integrates PCM beneath photovoltaic modules. Exploiting the latent heat absorption during the PCM phase transition, the system effectively moderates panel temperature. Three system configurations are assessed: uncooled photovoltaic panels, photovoltaic panels equipped with PCM, and photovoltaic panels incorporating both PCM and fins for enhanced thermal dissipation. Key performance indicators, including cell temperature, electrical output, and PCM liquid fraction, are evaluated across the set-ups. Results demonstrate a marked reduction in panel temperature with the use of PCM, while the addition of fins further amplifies cooling efficiency and electrical performance.

Key words: *photovoltaic cooling, PCM, thermal management, electrical efficiency, fin enhancement*

Introduction

Crystalline silicon photovoltaic (PV) modules are widely used in solar energy systems, yet their efficiency remains limited, only about 12%-18% of the incoming solar radiation is converted into electricity. The majority of the unused energy is converted into heat, which leads to an increase in module temperature and a subsequent decline in efficiency at a rate of approximately 0.4%-0.5% for every 1 °C rise in temperature [1, 2]. This thermal issue has prompted researchers to explore various cooling strategies to mitigate performance losses.

* Corresponding author, e-mail: mbayram34@gmail.com

Among the early efforts, active cooling techniques involving air or water circulation have led to the emergence of PV/thermal systems. Notable contributions in this area include those by Wolf [3], Kern Jr and Russell [4], Hendrie [5], and Raghuraman [6]. Further investigations have focused on optimizing air-flow conditions and geometric configurations to enhance heat dissipation and electrical output [7, 8]. Additional thermal analyses and experimental validations were carried out by Sopian *et al*. [9], Garg and Adhikari [10], Zondag *et al*. [11], Tiwari *et al*. [12], Solanki *et al*. [13], Baloch *et al*. [14], and Reteri *et al*. [15].

In recent years, passive cooling approaches, particularly the use of PCM, have attracted considerable interest. The PCM offer the advantage of absorbing excess heat through latent heat storage, thereby maintaining lower PV module temperatures and improving energy output stability [16]. Research in this domain has examined various aspects of PCM integration, including material selection, thermal conductivity enhancement, and optimal placement. Significant work has been reported by Qu *et al*. [17], Yagci *et al*. [18], Tang *et al*. [19], Sheikh *et al*. [20], Cai *et al*. [21], Meng *et al*. [22], and Shawish *et al.* [23].

The growing need for efficient thermal regulation in PV systems has driven interest in passive cooling strategies that enhance performance without additional energy consumption. Among these, the use of PCM offers a promising approach due to their ability to stabilize temperatures through latent heat absorption. This study is motivated by the potential of PCM-based cooling to mitigate thermal stress on PV modules and improve electrical efficiency under varying thermal loads. To further enhance heat dissipation, cooling fins are introduced to facilitate faster phase transitions.

Materials and methods

The studied PV solar collector consists of a 3 mm glass cover, a 0.3 mm polycrystalline silicon layer, and a 0.5 mm Tedlar backsheet, all mounted on a 1 mm aluminum casing that houses a 50 mm RT31 PCM layer, with the full module measuring 600 mm × 1200 mm. Three design configurations were analyzed: Case A (standard PV without cooling), Case B (PV with passive PCM cooling), and Case C (PV with PCM and aluminum fins for enhanced heat dissipation), with fin numbers varied at 7, 11, and 14, fig. 1. Internal fins of 1 mm thickness are used in some configurations to improve thermal regulation, see [24-26] for simulation property details.

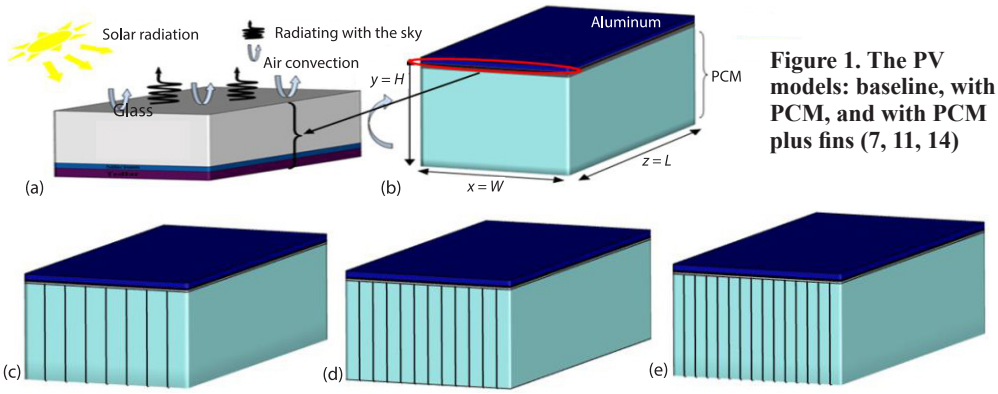

Figure 1. The PV models: baseline, with PCM, and with PCM plus fins (7, 11, 14)

The thermal analysis of the PVT/PCM system assumes 3-D heat transfer, with natural-convection in the liquid PCM modeled via the Boussinesq approximation. The PCM flow is considered Newtonian, incompressible, and laminar, while the material itself is treated as homogeneous and isotropic.

The PCM region's thermal behavior is modeled using modified conservation equations that include phase change and natural-convection, with mass conservation defined by the continuity equation. The mass conservation is expressed through the continuity equation:

$$\frac{\partial u}{\partial x}+\frac{\partial v}{\partial y}+\frac{\partial w}{\partial z}=0 \tag{1}$$

The x-direction momentum equation is given:

$$\frac{\partial\left(\rho_{\mathrm{PCM}}u\right)}{\partial t}+\nabla\left(\rho_{\mathrm{PCM}}Uu\right)=\nabla\left(\mu\nabla\mathrm{u}\right)-\frac{\partial p}{\partial x}+S_x \tag{2}$$

The y-momentum equation incorporates buoyancy using the Boussinesq approximation:

$$\frac{\partial\left(\rho_{\mathrm{PCM}}v\right)}{\partial t}+\nabla\left(\rho_{\mathrm{PCM}}Uv\right)=\nabla\left(\mu\nabla\mathrm{v}\right)-\frac{\partial p}{\partial y}+\rho\mathrm{g}\beta\left(T-T_{\mathrm{ref}}\right)+S_y \tag{3}$$

Similarly, the z-direction momentum equation is defined:

$$\frac{\partial\left(\rho_{\mathrm{PCM}}w\right)}{\partial t}+\nabla\left(\rho_{\mathrm{PCM}}Uw\right)=\nabla\left(\mu\nabla\mathrm{w}\right)-\frac{\partial p}{\partial x}+S_z \tag{4}$$

The energy conservation within the PCM is described by the modified thermal energy equation:

$$\rho_{\mathrm{PCM}}C_{p,\mathrm{PCM}}\left(\frac{\partial T}{\partial t}+u\frac{\partial T}{\partial x}+v\frac{\partial T}{\partial y}+w\frac{\partial T}{\partial z}\right)=\lambda_{\mathrm{PCM}}\left(\frac{d^2T}{\partial x^2}+\frac{d^2T}{\partial y^2}+\frac{d^2T}{\partial z^2}\right)+S_T \tag{5}$$

The PV electrical efficiency is estimated using an empirical correlation [27]:

$$\mu_C=0.125\left[1-0.004\left(T_{\mathrm{cell}}-293\right)\right] \tag{6}$$

These equations define velocity (u, v, and w), pressure, p, temperature, T, and material properties of the PCM ($C_{p,\mathrm{PCM}}$, λ_{PCM}), with source terms (S_x, S_y, and S_z) for phase change and an empirical relation, μ_C, for PV efficiency based on cell temperature.

To simulate the system's thermal behavior, suitable boundary and initial conditions were set. At the top boundary ($0\le x\le L$, $y=\mathrm{H}$, $0\le z\le l$, heat flux is defined:

$$\lambda\frac{\partial T}{\partial n}=G-h_{\mathrm{l}}\left(T_{\mathrm{g}}-T_{\mathrm{amb}}\right)-\varepsilon_{\mathrm{g}}\sigma\left(T_{\mathrm{g}}^4-T_{\mathrm{sky}}^4\right) \tag{7}$$

The convective coefficient h_{l} is based on Mac Adams' correlation:

$$h_{\mathrm{l}}=5.7+3.8V_{\mathrm{wind}} \tag{8}$$

For the four lateral edges of the PV panel, the boundary condition is given:

$$\lambda\frac{\partial T}{\partial n}=h_{\mathrm{l}}\left(T_{\mathrm{PV}}-T_{\mathrm{amb}}\right) \tag{23}$$

The thermal collector's side boundaries (air duct) are treated as adiabatic, with time-dependent solar radiation, ambient, and sky temperatures detailed in tab. 1.

The equations were solved using the SIMPLE algorithm [28] with Upwind discretization and the enthalpy-porosity method for melting. Relaxation factors and convergence criteria were set accordingly, with 20 iterations per time step. Mesh independence was verified using silicon layer temperature trends, and mesh sizes are listed in tab. 2. Time step sensitivity was analyzed using cell temperature trends, with 0.5 second chosen as optimal for all cases. Further details on model validation are provided in [24].

Table 1. Diurnal variation of key environmental parameters used in the simulation

Time	Sky temperature [K]	Asolar radiation intensity [Wm^{-2}]
8: 20 a. m.	278.85	255
9: 00 a. m.	279.20	375
9: 40 a. m.	279.50	483
10: 20 a, m.	279.90	575
11: 00 a. m.	280.10	650
11: 40 a. m.	280.30	705
12: 20 p. m.	280.60	736
13: 00 p. m.	280.75	750
13: 40 p. m.	280.83	736
14: 20 p. m.	280.83	705
15: 00 p. m.	280.75	650
15: 40 p. m.	280.60	576
16: 20 p. m.	280.30	484
17: 00 p. m.	280.10	376
17: 40 p. m.	279.80	257

Table 2. Mesh sizes for different system configurations

Adopted meshes	Configuration
109292 cells	PCM only
112240 cells	PCM with 7 fins
118800 cells	PCM with 11 fins
124600 cells	PCM with 14 fins

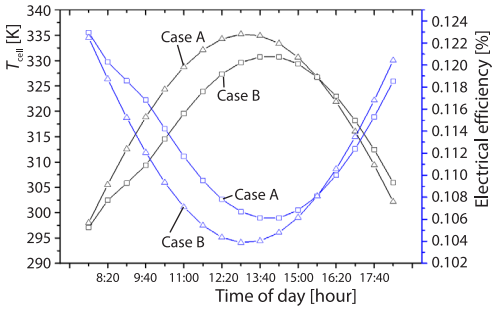

Figure 2. The PV temperature and efficiency over time with and without PCM

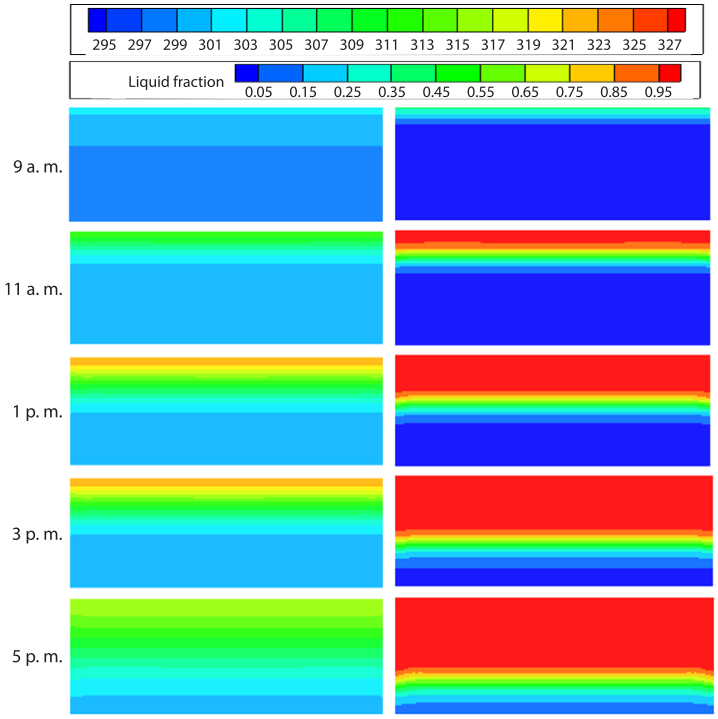

Figure 3. Daily Evolution of isotherms and liquid fraction for Case B (with PCM)

Results and discussions

Figure 2 shows the daily variation of silicon layer temperature and PV efficiency for Case A (without PCM) and Case B (with PCM). Both cases heat up with rising solar irradiance, peaking at 335.2 K (Case A, 1:00 p. m.) and 329.6 K (Case B, 1:40 p. m), demonstrating PCM ability to delay and reduce temperature rise. After 3:40 p. m., Case B's temperature slightly exceeds Case A due to heat release from the PCM. Efficiency drops as temperature increases, reaching 0.1038% (Case A) and 0.1062% (Case B). The PCM improves performance during peak hours, lowering temperature by ~6 °C and boosting efficiency by ~0.25% before 3:00 p. m. Later, Case A regains higher efficiency as it cools faster.

Figure 3 shows the daily evolution of isotherms and liquid fraction for Case B with PCM. Melting begins around 9:00 a. m. near the PV module as temperatures reach 303 K. By 11:00 a. m., about 23% of the PCM melts, increasing to 45% by 1:00 p. m. as temperatures peak near 323 K. At 3:00 p. m., the liquid fraction rises to 64%, and by 5:00 p. m., it reaches 76%, though full melting is not achieved. Heat transfer remains mainly conductive due to the PCM thin layer. This suggests performance could improve by adding conductive fins beneath the PV module.

Figure 4 shows the daily variation of silicon temperature and electrical efficiency for Case B, comparing PCM systems with and without fins. Fins enhance heat transfer, reducing PV cell temperature and delaying efficiency loss. Higher fin counts (14, 11, 7) lead to earlier PCM melting and better midday thermal control. After peak irradiance (~4:20 p. m.), finned systems release stored heat more slowly, temporarily raising temperatures above the non-finned case. Overall, fins lower peak temperatures by ~15 °C and improve efficiency by ~0.6% during peak hours (11:00 a. m. to 3:00 p. m.), with higher fin densities offering better performance.

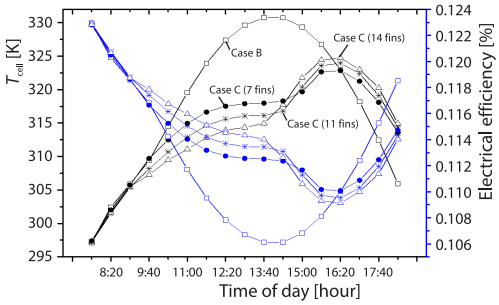

Figure 4. Silicon temperature and electrical efficiency *vs.* time for Case B with/without fins

Figures 5 and 6 present the temperature contours and liquid fraction distributions throughout the day, respectively. In these figures, blue indicates solid PCM regions ($f_l = 0$), red denotes fully melted regions ($f_l = 1$), and the gradient colors represent the mushy zone ($0 < f_l < 1$). At 9:00 a. m., the PCM temperature near the upper section adjacent to the PV module reaches between 301 K and 303 K in the 7 fin configuration, falling within the phase change range and indicating the onset of melting. For the 11 fin case, the maximum temperature is approximately 301 K, initiating minimal melting, while the 14 fin configuration peaks at 299 K, with the PCM remaining entirely solid. This behavior is attributed to the increased aluminum mass and improved heat distribution as the number of fins rises.

By 11:00 a. m., the PCM temperature in the upper region of the 7 fin configuration increases to about 304 K, corresponding to a liquid fraction of roughly 14%. In comparison, the PCM temperature in the 11 fin and 14 fin configurations reaches around 304 K throughout the entire volume, driven by the enhanced heat transfer surface area. As a result, the liquid fractions increase to 19% and 25% for the 11 fin and 14 fin cases, respectively.

Between 1:00 p. m. and 5:00 p. m., the PCM temperature continues to rise with the number of fins, reaching peak values of approximately 318 K, 319 K, and 320 K for the 7 fin, 11 fin, and 14 fin configurations, respectively. At 3:00 p. m., liquid fraction analysis indicates complete melting in the 14 fin configuration, while the 11 fin and 7 fin cases reach melting lev-

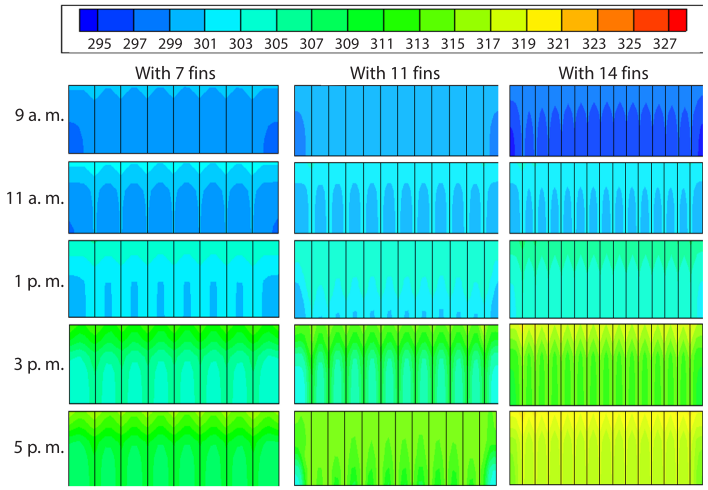

Figure 5. Temperature contours of PCM throughout the day for different fin configurations

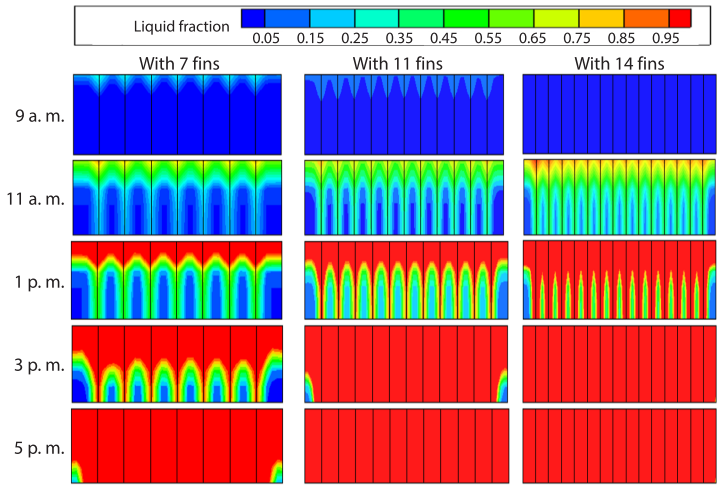

Figure 6. The PCM liquid fraction over the day for various fin configurations

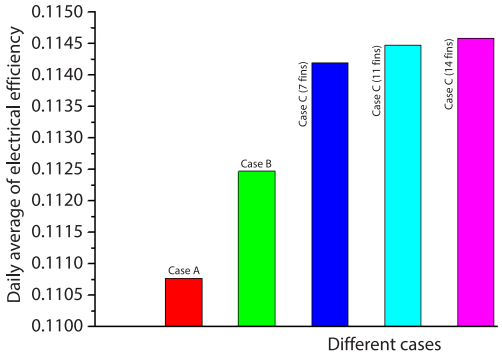

Figure 7. Average electrical efficiency for different PCM and fin configurations

els of approximately 97% and 76%, respectively. By 5:00 p. m., complete melting is observed in the 11-fin configuration, whereas the 7 fin PCM achieves a melting level of about 98.5%.

Figure 7 illustrates the average electrical efficiency for the various cases under investigation. In Case B, the integration of the PCM results in a noticeable enhancement in electrical efficiency, with an average increase of 0.17% compared to the baseline Case A. The addition of fins in Case C further augments this improvement, yielding an average gain of 0.17% over Case B and a total enhancement of 0.34% relative to Case A.

For the finned PCM configurations, a clear trend is observed: increasing the number of fins improves the cooling effectiveness of the PV cells, thereby leading to higher electrical efficiencies. This is attributed to the enhanced heat transfer facilitated by the greater surface area provided by the fins. The figure also confirms that each successive thermal management strategy contributes positively to overall performance. The highest electrical efficiency is achieved in Case C with 14 fins, demonstrating the effectiveness of this configuration in optimizing thermal regulation and maximizing photovoltaic output.

Conclusion

This study conducts a theoretical analysis of PV module thermal regulation through the application of PCM. It explores the thermal and electrical performance of PV panels equipped with PCM cooling systems in comparison conventional, non-cooled counterparts. To intensify the heat transfer process, fins were embedded within the PCM structure, with particular attention given to the effect of fin quantity on thermal dynamics. The numerical findings reveal that PCM integration can reduce the surface temperature of PV cells by approximately 5-6 °C during periods of maximum solar irradiance, thereby yielding a modest electrical efficiency gain of around 0.2%. Notably, the addition of fins within the PCM substantially enhances heat dissipation by accelerating the phase transition. This design enhancement leads to an improved thermal response, with temperature reductions reaching 13-14 °C beyond those observed in systems lacking fins.

References

[1] Ingersoll, J. G., Simplified Calculation of Solar Cell Temperatures in Terrestrial Photovoltaic Arrays, *J. Sol. Energy Eng*., *108* (1986), 2, pp. 95-101
[2] Krauter, S., *et al.*, Simulation of Thermal and Optical Performance of PV Modules – Part III: *Renew. Energy*, *5* (1994), 3, pp. 1701-1703
[3] Wolf, M., Performance Analyses of Combined Heating and Photovoltaic Power Systems for Residences, *Energy Conversion*, *16* (1976), 1-2, pp. 79-90
[4] Kern Jr, E. C., Russell, M. C., Combined Photovoltaic and Thermal Hybrid Collector Systems (No. COO-4577-3; CONF-780619-24), Lincoln Lab., Massachusetts Inst. of Tech., Lexington, Mass., USA, 1978
[5] Hendrie, S. D., Evaluation of Combined Photovoltaic/Thermal Collectors (No. COO-4577-8; CONF-790541-54), Lincoln Lab., Massachusetts Inst. of Tech., Lexington, Mass., USA, 1979
[6] Raghuraman, P., Analytical Predictions of Liquid and Air Photovoltaic/Thermal, Flat-Plate Collector Performance, *J. Sol. Energy Eng*., *103* (1981), 4, pp. 291-298
[7] Bhargava, A. K., *et al.*, Study of a Hybrid Solar System – Solar Air Heater Combined with Solar Cells, *Energy Conversion and Management*, *31* (1991), 5, pp. 471-479
[8] Prakash, J., Transient Analysis of a Photovoltaic-Thermal Solar Collector for co-Generation of Electricity and Hot Air/Water, *Energy Conversion and Management*, *35* (1994), 11, pp. 967-972
[9] Sopian, K., *et al*., An Investigation into the Performance of a Double Pass Photovoltaic Thermal Solar Collector, *Procedings*, ASME Int. Mechanical Engineering Congress and Exhibition, San Francisco, Cal., USA, 1995, Vol. 35, pp. 89-94
[10] Garg, H. P., Adhikari, R. S., Performance Analysis of a Hybrid Photovoltaic/Thermal (PV/T) Collector with Integrated CPC troughs, *International Journal of Energy Research*, *23* (1999), 15, pp. 1295-1304
[11] Zondag, H. A., *et al*., PVT Roadmap, A European Guide for the Development and Market Introduction of PVT Technology, Rapport EU-Project PV-Catapult, 2005, p. 87
[12] Tiwari, A., *et al*., Performance Evaluation of Photovoltaic Thermal Solar Air Collector for Composite Climate of India., *Solar Energy Materials and Solar Cells*, *90* (2006), 2, pp. 175-189
[13] Solanki, S. C., *et al*., Indoor Simulation and Testing of Photovoltaic Thermal (PV/T) *air collecto*rs, *Applied Energy*, *86* (2009), 11, pp. 2421-2428
[14] Baloch, A. A., *et al*., Experimental and Numerical Performance Analysis of a Converging Channel Heat Exchanger for PV Cooling, *Energy Conversion and Management*, *103* (2015), Oct., pp. 14-27
[15] Reteri, A., *et al.*, Experimental Study of Temperature Influence on the Electrical Performance of Polycrystalline Photovoltaic Cell, *Mechanics & Mechanical Engineering*, *22* (2018), 4, pp. 1111-1119

[16] Korti, A. I. N., Numerical Heat Flux Simulations on Double-Pass Solar Collector with PCM Spheres Media, *International Journal of Air-Conditioning and Refrigeration*, *24* (2016), 02, 1650010
[17] Qu, H., *et al*., Experimental Study on the Effect of Tilt Angle on the Output Parameters of a Photovoltaic-Phase Change Material (PV-PCM) System under Wind Conditions, *Journal of Energy Storage*, *102* (2024), 114263
[18] Yagci, O. K., *et al*., An Experimental Study on the Performance of PCM-Based Heat Sink with Air for Thermal Regulation of PV, *Solar Energy*, *278* (2024), 112800
[19] Tang, H., *et al*., Experimental Study of a PV-PCM Window under Hot Summer and Warm Winter Climate, *Journal of Energy Storage*, *96* (2024), 112724
[20] Sheikh, Y., *et al*., Enhancing PV Solar Panel Efficiency through Integration with a Passive Multi-Layered PCM Cooling System: A Numerical Study, *International Journal of Thermofluids*, *23* (2024), 100748
[21] Cai, H., *et al.*, Thermally Geometric Design of Phase Change Material and Photovoltaic (PV-PCM) for Cooling and Efficiency Improvement, *Renewable Energy*, *254* (2025), 123533
[22] Meng, E., *et al.*, Study on Simulation and Optimization of Thermal Performance of PV-PCM Roof in China, *International Communications in Heat and Mass Transfer*, *166* (2025), 109145
[23] Shawish, H., *et al*., Performance Investigation and Machine Learning Modelling of PV Panels Equipped with PCM Based Passive Cooling Systems, *Applied Thermal Engineering*, *274* (2025), 126588
[24] Reteri, A., Korti, N. A. I., Computational Analysis of Phase Change Material and Fins Effects on Enhancing PV/T Panel Performance, *Journal of Mechanical Science and Technology*, *31* (2017), July, pp. 3083-3090
[25] ***, Rubitherm, Technologies, Innovative PCM's and Thermal Technology, Product Manual RUBITHERM 2009, SP22A17
[26] Sarhaddi, F., *et al*., An Improved Thermal and Electrical Model for a Solar Photovoltaic Thermal (PV/T) Air Collector, *Applied Energy*, *87* (2010), 7, pp. 2328-2339
[27] Bergene, T., Lovvik, O. M., Model Calculations on a Flat-Plate Solar Heat Collector with Integrated Solar cells, *Solar Energy*, *55* (1995), 6, pp. 453-462
[28] Patankar, S., *Numerical Heat Transfer and Fluid-Flow*, CRC Press, Boca Raton, Fla., USA, 2018

Paper submitted: March 2, 2025
Paper revised: May 4, 2025
Paper accepted: July 10, 2025